Three-dimensional Particle Acceleration in Electromagnetic Dominated Outflows with Background Plasma and Clump

Koichi Noguchi and Edison Liang

Rice University, Houston, TX 77005-1892

(Dated: September 11, 2006)

Abstract

The effect of background plasma on particle acceleration via Poynting fluxes is studied in 3D PIC simulation of electron-positron and electron-ion plasmas. When a strongly magnetized ejecta at the center expands to low-temperature electron-positron ambient plasma background and a low-density clump, electromagnetic wave front accelerates particles in the background and clump, and captures them in the Ponderomotive potential well. We do not observe any instability, and the momentum distributions of background and clump form a power law of slope close to -1.5 with a sharp peak in the middle. When an ejecta expands to the ion-electron interstellar medium (ISM), the acceleration via Poynting flux is severely damped due to the charge separation.

Keywords: gamma rays:bursts—MHD—methods:numerical—relativity

I. INTRODUCTION

Gamma-ray bursts (GRBs) are the most luminous physical phenomenon in the universe, whose mechanism is still unknown. There are two competing paradigms for the origin of the prompt GRB emissions: hydrodynamic internal shocks [6, 9] versus Poynting fluxes[5]. Both pictures require the rapid and efficient acceleration of nonthermal electrons to high Lorentz factors in moderate magnetic fields to radiate gamma-rays. In the hydrodynamic internal shock scenario, shock wave energy is mainly transferred to ions, resulting emission with low energy peak, whereas in the Poynting flux scenario, long-wavelength electromagnetic (EM) energy can be directly converted into gamma-rays using the electrons or electron-positron pairs as radiating agents.

Recent large-scale 3D PIC simulations[2, 7] shows that relativistic jets propagating through a weakly or nonmagnetized ambient plasma exite the Weibel instability, and that accelerated electron jet in the electron-ion jet has a significant hump above a thermal distribution, whereas electron-positron jet does not. However, the maximum γ is around 10 in both cases, and acceleration mainly occurs in the perpendicular direction relative to the shock wave propagation.

The recent 2D PIC simulations[3, 4], which is particularly relevant to the Poynting flux scenario of GRBs, shows that intense EM pulses imbedded in an overdense plasma (EM wavelength $\lambda \gg$ plasma skin depth c/ω_{pe}) capture and accelerate particles via sustained in-phase Lorentz forces when the EM pulses try to escape from the plasma. Such Poynting flux may originate as hoop-stress-supported magnetic jets driven by strongly magnetized accretion onto a nascent blackhole, or as transient millisecond magnetar winds, in a collapsar event[13] or in the merger of two compact objects[10].

Liang & Nishimura [4] showed that the Poynting flux acceleration (PFA) reproduces from first-principles many of the unique features of GRB pulse profiles, spectra and spectral evolution, and Noguchi et. al.[8] recently showed that the mechanism is robust even with the radiation damping force.

In this article we report 3D PIC simulations of particle acceleration driven by Poynting flux with low-temperature background ambient medium and low-density clump with newly developed 3D PIC code, and we show the power spectrum and radiation power strength from each particle.

II. INITIAL SETUP OF THE SIMULATION

We use the 3D explicit PIC simulation scheme based on the Yee algorithm[12]. Spatial grids for the fields are uniform in all directions, $\Delta x = \Delta y = \Delta z = c/\omega_{pe}$, where ω_{pe} is the electron plasma frequency. The simulation domain is $-600\Delta x \leq x \leq 600\Delta x$, $-5\Delta y \leq y \leq 5\Delta y$ and $-5\Delta z \leq z \leq 5\Delta z$ with triply periodic boundary conditions.

Following Noguchi et. al.[8], the background magnetic field $\boldsymbol{B}_0 = [0, B_y, 0]$ is applied at the center of the simulation box, $-6\Delta x < x < 6\Delta x$, $-5\Delta y \leq y \leq 5\Delta y$ and $-5\Delta z \leq z \leq 5\Delta z$, so that the magnetic field freely expands toward the ambient plasma regions. The magnetic field strength B_y is given by

$$B_y = \begin{cases} B_0, & |x| < 4\Delta x \\ B_0[-|x|/(2\Delta x) + 3], & 4\Delta x < |x| < 6\Delta x \\ 0, & \text{otherwise} \end{cases} . \tag{1}$$

We note that B_y has finite gradient at edges to avoid unphysical particle acceleration.

In order to study the particle acceleration only from PFA, initial electric field and current are assumed to be zero, which seems rather too simple and artificial. However, our study shows[8] that the acceleration is insensitive to the initial field configuration, and the existence of ordered Poynting vector is the key to accelerate particles via PFA. The group velocity of EM wave front is very close to the speed of light, and any hydrodynamical instability due to the electric field or current non-uniformity can be ignored. The most energetic particles are concentrated in the wave front, and instabilities such as Weibel instability which may occur in downstream does not affect the PFA mechanism.

The number density distribution of initial electron-positron ejecta ρ_{ej} is proportional to B_y in order to keep the ratio $\omega_{pe}/\Omega_{ce} = 0.1$, where Ω_{ce} is the electron cyclotron frequency.

The clump and the ambient plasma consist of either electron-positron or electron-ion. The clump is a $100\Delta x \times 6\Delta y \times 6\Delta z$ cuboid with density $\rho_{cl} = 0.1\rho_{ej}$, whose center is located at $(-60\Delta x, 0, 0)$ so that the distance between the front of the ejecta and the edge of the column is $4\Delta x$. The remaining of the simulation box is filled by the ambient plasma with density $\rho_{am} = 0.01\rho_{ej}$.

The initial temperature of ejecta is assumed to be a spatially uniform relativistic Maxwellian, $k_B T_e = k_B T_p = 1\text{MeV}$, where the subscripts e and p refer to electrons and positrons. The temperature of the clump and the ambient plasma is also uniform Maxwellian

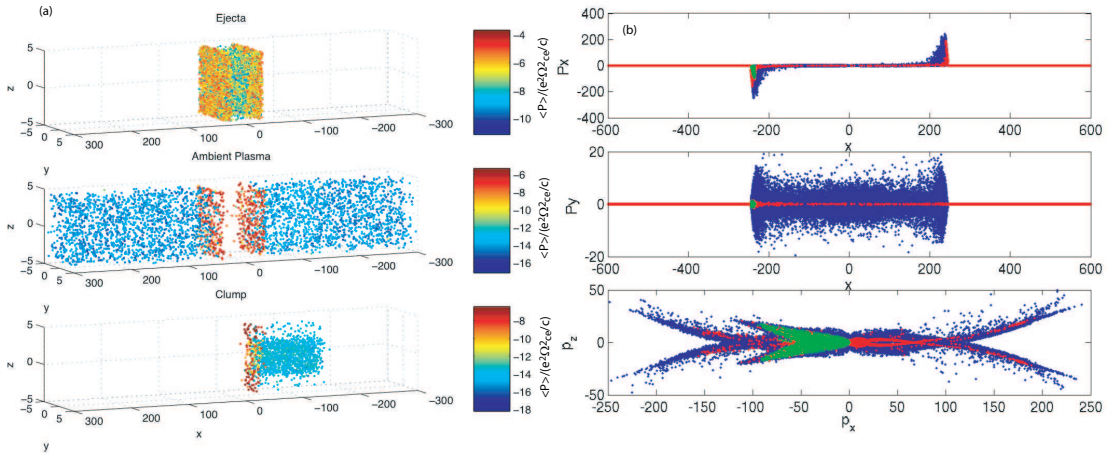

FIG. 1: The spatial distribution of particles in the ejecta (top), ambient medium (middle) and clump (bottom) at $t\Omega_{ce} = 650$, and the phase plot of particles at $t\Omega_{ce} = 12000$ with $P_x - x$ (top), $P_y - x$ (middle) and $P_z - P_x$ (bottom). The color of each particle in the left panel represents the magnitude of estimated radiation damping power $\langle P \rangle$. In the right panel, blue dots represent ejecta particles, green clump, and red ambient, respectively.

with $k_B T_e = k_B T_{p,i} = 100\text{eV}$.

III. RESULTS

First, we study the electron-positron background case. Figure 1 shows the spatial distribution of particles at $t\Omega_{ce} = 650$ and the phase plot at $t\Omega_{ce} = 12000$. The color of each particle in Fig. 1*a* represents the magnitude of estimated radiation damping force using the relativistic dipole formula [11]

$$\langle P \rangle = \frac{2e^2}{3m^2c^3}(F_\parallel^2 + \gamma^2 F_\perp^2), \tag{2}$$

where $F_\parallel$ and $F_\perp$ are the parallel and perpendicular components of the force with respect to the particle's velocity.

As the ejecta expands, electric field is automatically generated in the z direction, expanding the clump in the z direction. Particles are also accelerated in the direction of the Poynting vector (positive x direction for $x > 0$ and negative for $x < 0$), due to the ponderomotive force. At $t\Omega_{ce} = 12000$, acceleration by PFA still continues, and the clump is compressed into a thin layer co-moving with the wave front. Figure 1*b* shows that the

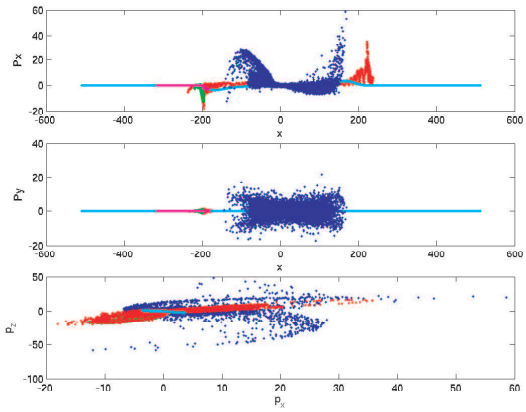

FIG. 2: The phase plot of electrons with ISM plasma ($x > 0$) and with ion-electron clump and ISM ($x < 0$) at $t\Omega_{ce} = 10000$ with $P_x - x$ (top), $P_y - x$ (middle) and $P_z - P_x$ (bottom). The meaning of colors is the same as Fig. 1.

highest γ in the ejecta is around 250, whereas $\gamma \simeq 100$ in the background and the clump. As we mentioned, there is no acceleration in the y direction, and the momentum distribution in the y direction does not change. There is no charge separation in the x direction, and no instability occurs in front of the EM pulse.

Figure 2 shows the phase plot of electrons in the ion-electron clump and ambient plasma case at $t\Omega_{ce} = 3000$. Different from the electron-positron case, the acceleration by the PFA is strongly reduced by the charge separation. Especially with the clump ($x < 0$), the initial EM field energy is too weak to accelerate ions, and electrons are bounced back to the center. However, electrons in the wavefront ($x \simeq \pm 300$) are still captured by the pontderomotive force well, and accelerated by PFA.

Next, we compare the power spectrum of electrons in both runs at $t\Omega_{ce} = 3000$. Figure 3a shows the electron-positron case and Figure3b shows the electron-ion case with the clump (C) and without the clump (NC). In the electron-positron case, the existence of clump does not affect the acceleration of the ejecta. Particles in both clump and ambient plasma get acceleration, making a sharp peak at $E = 1.2mc^2$, and form a power law of slope close to -1.5. The ion-electron case shows that the energy peak of the ambient plasma shifts to the lower, and the acceleration of the ejecta is severely reduced because of the charge separation between ions and electrons even though the ejecta consists of electrons and positrons. The power spectrum for the clump and background plasma sharply drops

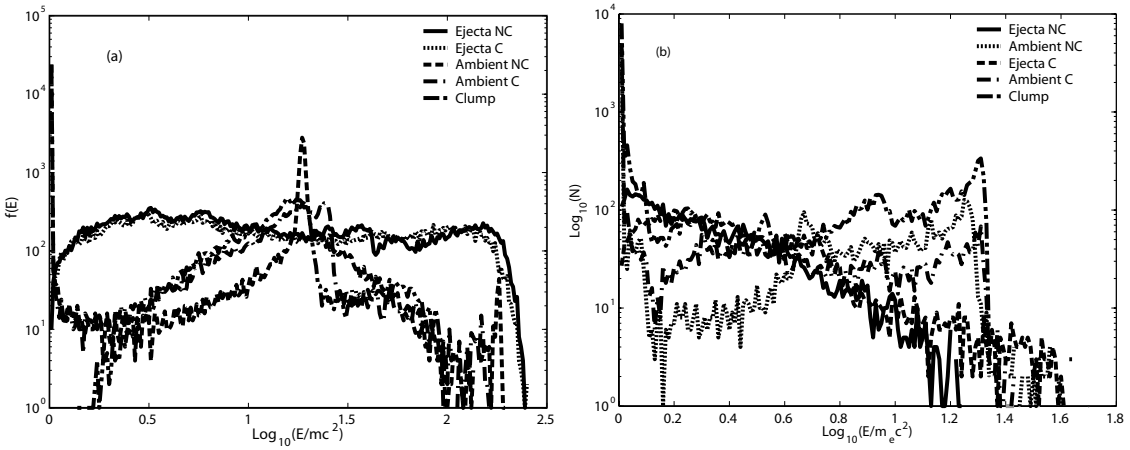

FIG. 3: The power spectrum of electrons in the electron-positron case (a) and the ion-electron case (b).

around $E = 1.3mc^2$, indicating that the electric field by the charge separation slows down the accelerated particles.

IV. SUMMARY

We studied the effect of electron-positron and ion-electron background ambient plasma on particle acceleration via Poynting fluxes. With electron-positron ambient plasma, the acceleration mechanism is still robust in the electron-positron background case, and particles in the background and clump are also accelerated. With the ion-electron case, however, the acceleration is severely suppressed due to the charge separation in the background and clump plasma. If the density of interstellar medium near the ejecta is more than 10%, higher initial magnetic field energy $\omega_{pe}/\Omega_{ce} \gg 1$ is required to create high energy tail by PFA.

The advantage of PFA compared with the internal shock acceleration scenario is the efficient energy transfer to high energy particles, and less bulk heating. High energy tail of GRBs requires $gamma > 100$ or more, which can be explained by the energetic particles accelerated by PFA, but not by the internal shock. When electron-positron and electron-ion plasma coexist, charge separation between ions and electrons decelerates the acceleration. Internal shock acceleration may take place if the initial plasma temparature is so low that ion density is much higher than positron density, or the initial plasma is weakly or not magnetized. We are currently working on simulations of the electron-positron with low-

density electron-ion plasma in the ejecta and background.

Longer timescale simulations are required to show the final power distribution of particles and resulting radiation spectrum, which remains as a future problem.

Acknowledgments

This research is partially supported by NASA Grant No. NAG5-9223, NSF Grant No. AST0406882, and LLNL contract nos. B528326 and B541027. The authors wish to thank ILSA, LANL, B. Remington and S. Wilks for useful discussions.

---

[1] Birdsall, C. K., Langdon, A. B.: Plasma Physics via Computer Simulation, McGraw-Hill, 1985

[2] Hededal, C. B., Nishikawa, K.-I.: ApJ, **623**, L89 (2005)

[3] Liang, E., Nishimura, K., Li, H., Gary, S. P.: Phys. Rev. Lett., **90**, 085001 (2003)

[4] Liang, E., Nishimura, K.:Phys. Rev. Lett., **92**, 175005 (2004)

[5] Lyutikov, M., Blackman, E. G.: MNRAS, **321**, 177 (2001)

[6] Mészáros, P.: Annual Review of Astronomy and Astrophysics, **40**, 137 (2002)

[7] Nishikawa, K.-I., Hardee, P. E., Hededal, C. B., Fishman, G. J.:ApJ, **642**, 1267 (2006)

[8] Noguchi, K., Liang, E., Nishimura, K.: Nuovo Ciment C, **028**, 381 (2005)

[9] Piran, T.: Phys. Repts. **33**, 529 (2000)

[10] Ruffert, M., Janka, H-Th.: Gamma-Ray Burst and Aftergrow Astronomy, AIP Conference Proceedings, **662**, 193 (2003)

[11] Rybicki, G. B., Lightman, A. P.: Raidiative Processes in Astrophysics, Wiley-interscience, New York, 1979

[12] Yee, K. S.: IEEE Trans. Antennas Propag., **14**, 302 (1966)

[13] Zhang, W., Woosley, S. E., MacFadyen, A. I.: ApJ, **586**, 356 (2003)